

Anomalous Thermoelectric Transport of Dirac Particles in Graphene

Peng Wei, Wenzhong Bao, Yong Pu, Chun Ning Lau, and Jing Shi

Department of Physics and Astronomy, University of California, Riverside, California 92521, USA

(Received 12 December 2008; published 24 April 2009)

We report a thermoelectric study of graphene in both zero and applied magnetic fields. As a direct consequence of the linear dispersion of massless particles, we find that the Seebeck coefficient S_{xx} diverges with $1/\sqrt{|n_{2D}|}$, where n_{2D} is the carrier density. We observe a very large Nernst signal S_{xy} ($\sim 50 \mu\text{V}/\text{K}$ at 8 T) at the Dirac point, and an oscillatory dependence of both S_{xx} and S_{xy} on n_{2D} at low temperatures. Our results underscore the anomalous thermoelectric transport in graphene, which may be used as a highly sensitive probe for impurity bands near the Dirac point.

DOI: 10.1103/PhysRevLett.102.166808

PACS numbers: 73.23.-b, 72.15.Gd, 72.15.Jf, 73.50.Lw

The unusual band structure of graphene gives rise to a host of intriguing phenomena in electrical transport properties that have been under extensive experimental investigations [1–6]. In solids, both charge and heat flows are simultaneously generated when an electrochemical potential or a temperature gradient is present, leading to additional effects. Fundamentally related to the electrical conductivity, other transport coefficients such as thermal conductivity and thermoelectric coefficients are also determined by the band structure and scattering mechanisms. Thermoelectric coefficients, in particular, involve the energy derivatives of the electrical transport counterparts such as the conductivity σ and the Hall angle Θ_H . The anomalies in the latter are very often amplified and cause markedly distinct features in the former near the Dirac point. Furthermore, in the regime where the Mott relation is applicable, the relationship between the measured electrical conductivity and the Seebeck coefficient reveals how the chemical potential depends on the gate voltage or carrier density, which is dictated by the energy dispersion. Therefore, the thermoelectric transport coefficients can offer unique information and are complementary to the electrical transport coefficients. A number of theoretical predictions have been made on transport coefficients other than electrical conductivities in graphene [7–9] which to date remain experimentally unexplored.

Single-layer graphene sheets are mechanically exfoliated onto degenerately doped silicon substrates that are covered with 300 nm of silicon dioxide. After locating suitable graphene sheets, we perform standard electron-beam lithography to attach electrodes in Hall-bar geometry. The electrodes consist of 7 nm of Cr and 100 nm of Au, and also serve as local thermometers. A microfabricated heater located on the right of Fig. 1(a) generates nearly parallel constant temperature contours along the graphene sample. The thermal voltage generated is measured across the two parallel Cr/Au electrodes $\sim 20 \mu\text{m}$ apart. These also double as local thermometers whose resistance is measured by the four-point method. A temperature difference of $\sim 10 \text{ mK}$ between the two Cr/Au wires can be readily measured for temperature $T > 10 \text{ K}$. An additional

pair of Cr/Au leads is used for transverse (Hall or Nernst) voltage measurements. All measurements were carried out in a cryostat with T ranging from 1.5 to 300 K and magnetic field B up to 8 T. In this work, the results are from two representative devices (#1 and #2) out of approximately two dozen fabricated devices. They are single-layer graphene as determined from optical images, and are often corroborated by the well-defined half-integer quantum Hall effect at low temperature. The carrier mobility μ_c is typically $\sim 3000 \text{ cm}^2/\text{V s}$.

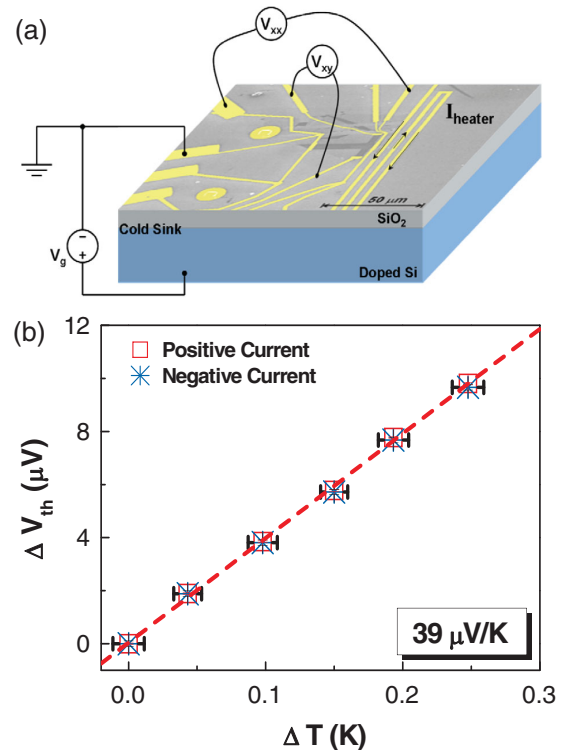


FIG. 1 (color). (a) SEM image and circuit schematic of a graphene device for thermoelectric measurements. (b) ΔT vs thermovoltage change ΔV_{th} for a series of heater power steps at 255 K and zero gate voltage. The linear fit of this curve gives the thermopower of $39 \mu\text{V}/\text{K}$.

We generate a temperature gradient and measure both the temperature difference ΔT and thermal voltage change ΔV_{th} . Fitting a straight line to the ΔV_{th} vs ΔT data, we extract the Seebeck coefficient $S_{xx} = -\frac{\Delta V_{\text{th}}}{\Delta T}$ from the slope [Fig. 1(b)] [10]. At zero magnetic field, σ exhibits the characteristic minimum at $V_g \sim V_D$, the Dirac point. Figure 2(a) shows V_{th} as a function of V_g for three temperatures. V_{th} undergoes a sign change at the Dirac point $V_g = V_D = 10$ V, indicating the carrier type changes from hole to electron as $V_g - V_D$ is swept from negative to positive. V_{th} has a finite slope near V_D over a 20 V range in V_g which corresponds to $\sim \pm 100$ meV change in chemical potential μ measured from the Dirac point. This region coincides with the minimum in σ , where charged impurities modify the conductivity [11–14]. As V_g is further away from V_D on both sides, the magnitude of V_{th} decreases, scaling approximately with $1/\sqrt{|V_g - V_D|}$ [dashed line in Fig. 2(a)]. This V_g dependence is more noticeable in the linear dependence of $1/V_{\text{th}}^2$ on V_g [Fig. 2(b)]. The dashed lines are the power-law fits with exponent ~ 0.95 and cross zero in the vicinity of the Dirac point from both sides, indicating a diverging behavior of S_{xx} . Note that near the Dirac point, V_{th} crosses zero, and the $1/\sqrt{|V_g - V_D|}$ dependence breaks down, as denoted by the hatched region. For comparison, the same V_{th} data are also plotted as $1/|V_{\text{th}}|$ vs V_g in Fig. 2(c), and the straight lines are drawn in the linear region. Clearly, the $1/V_{\text{th}}^2$ plot shows a better linear relationship with V_g over the whole range. In addition, $1/V_{\text{th}}^2$ extrapolates to zero at almost the same V_g for different temperatures, but $1/|V_{\text{th}}|$ does not.

The fact that $|V_{\text{th}}|$ or $|S_{xx}|$ diverges as $1/\sqrt{|V_g - V_D|}$ is actually a direct manifestation of the linear dispersion of the Dirac particles in graphene. Let us assume $\sigma \sim |\mu|^\alpha$, which is sufficiently general to include both dirty ($\alpha \sim 2$) and clean ($\alpha \sim 1$) limits [12,13]. For degenerate electron systems, we expect the Mott relation $S_{xx} = -\frac{\pi^2 k_B^2 T}{3e} \frac{\partial \ln \sigma(\mu)}{\partial \mu}$ to hold, yielding $S_{xx} \sim -\frac{1}{\mu}$ for highly doped regimes. On the other hand, for a 2D system with a linear dispersion relation, then we expect $\mu = \hbar v_F \sqrt{n_{2D} \pi} \propto \pm \sqrt{|V_g - V_D|}$, where the $+$ ($-$) sign corresponds to the electron- (hole-) doped regime, and v_F is the Fermi velocity. Combining these relations, we have $S_{xx} \sim \frac{-\text{sgn}(\mu)}{\sqrt{|V_g - V_D|}}$. This is in contrast to the ordinary 2D electron systems with a quadratic dispersion relation, in which $\mu \propto n_{2D}$, and hence $S_{xx} \sim \frac{-1}{V_g - V_D}$. From this diverging behavior of S_{xx} , we can conclude that the dispersion relation is linear rather than quadratic, as expected for Dirac particles. It is worth noting that the exponent α is absorbed in the prefactor of S_{xx} and does not affect the functional dependence of S_{xx} , as is the case in σ . This makes the thermoelectric transport uniquely sensitive to the electronic band structure.

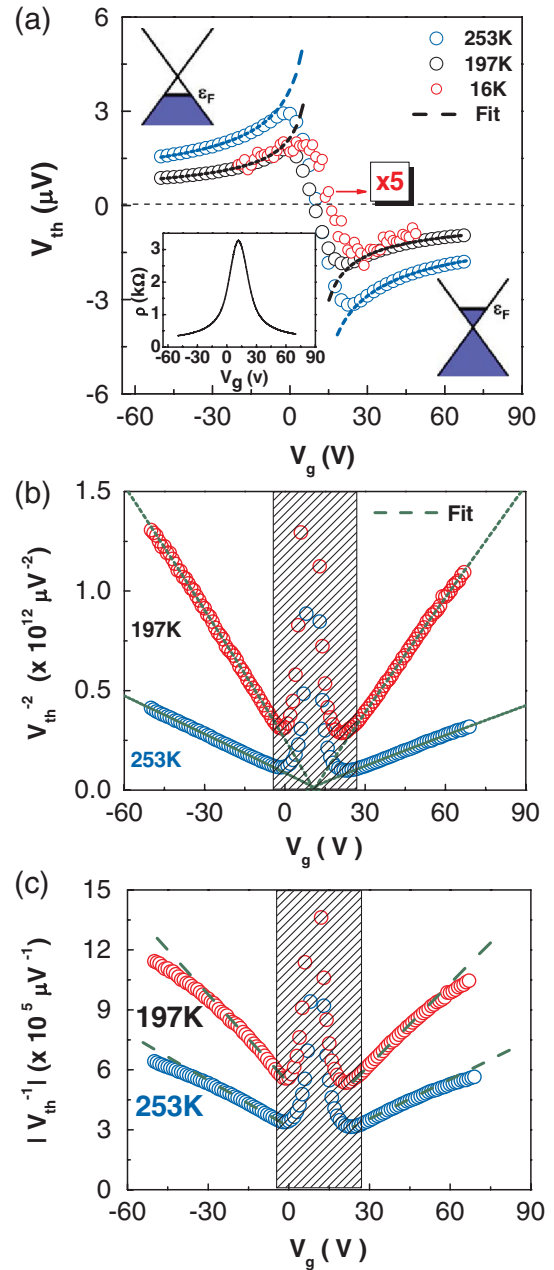


FIG. 2 (color). (a) V_{th} vs V_g for three different temperatures. The 16 K data (red circle) were multiplied by a factor of 5. The dashed lines are the fits described by $|S_{xx}| \sim 1/\sqrt{|V_g - V_D|}$. (b) $1/V_{\text{th}}^2$ vs V_g plot for the same data shown in (a). The shaded area is for $|V_g - V_D| < 10$ V. Green dashed lines are the best power-law fits with exponent ~ 0.95 . (c) $1/|V_{\text{th}}|$ vs V_g plot for the same data in (a). Green dashed lines are straight lines as guides to the eye.

Not every device shows the electron-hole symmetry shown in Fig. 2. Figure 3(a) displays S_{xx} vs V_g of a different device with $V_D \sim 33$ V for several values of T ranging from 11 to 255 K. Away from V_D on the hole side, S_{xx} decreases with decreasing V_g , similar to the behavior of the previous device. In contrast, S_{xx} stays flat on the electron side, indicating a strong electron-hole asymmetry as seen

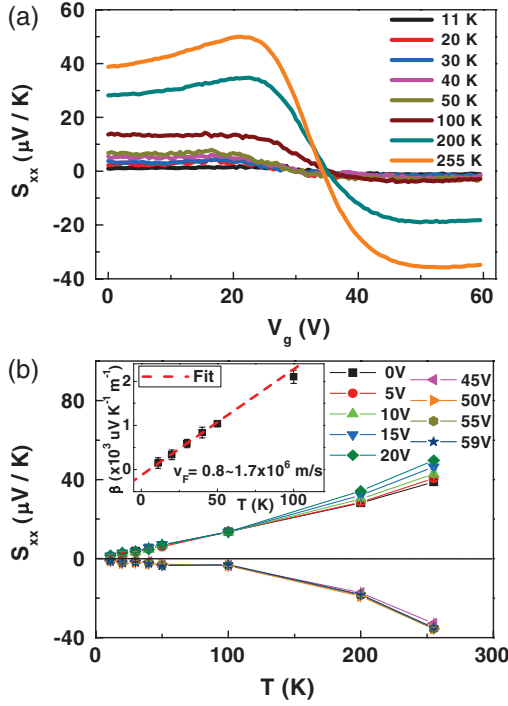


FIG. 3 (color). (a) V_g dependence of longitudinal Seebeck coefficient S_{xx} at different temperatures (11–255 K) and zero magnetic field. (b) T dependence of S_{xx} at different gate voltages. The inset is the T dependence of $\beta = S_{xx}\sqrt{n_{2D}}$ at $V_g = 0$ V for low temperatures. The slope of the linear fit is proportional to α/v_F .

in σ by others [12]. Near V_D , we observe a broad transition region in S_{xx} connecting the electron- to hole-doped regimes. Furthermore, S_{xx} follows different T dependence for different V_g [in Fig. 3(b)]. Near V_D , the magnitude of S_{xx} is close to zero. Away from V_D on the hole side, e.g., at $V_g = 0$ V or ~ 33 V left of V_D , S_{xx} is nearly a straight line for the whole temperature range. As V_g approaches V_D from the hole side, S_{xx} begins to deviate from the linear T dependence at progressively lower temperatures. On the electron side, however, even at $V_g = 60$ V (or ~ 30 V right of V_D), S_{xx} remains nonlinear in T except at very low temperatures.

The departure from the linear T dependence is an indication of the potential breakdown of the Mott relation. For this device, when $|V_g - V_D| = 30$ V, $|\mu|$ is about 160 meV measured from the Dirac point. It is reasonable to expect high-order corrections in the Sommerfeld expansion at relatively high temperature where the condition $|\mu| \gg k_B T$ fails. For graphene, another relevant energy scale is the bandwidth γ of impurity states [15,16] near the Dirac point. The Mott relation only holds if $\frac{\gamma}{k_B T} \gg 1$, which ensures σ to be a slow-varying function of energy over this band of impurity states [16]. In the impurity scattering model, this band can be highly asymmetric due to the finite scattering potential. Here, we attribute the departure from the linear T dependence on the electron

side to the asymmetric nature of the band of impurity states. For this reason, we only focus on the relatively low- T region on the hole side where the Mott relation apparently holds. Since S_{xx} is proportional to αT , and inversely proportional to μ or $v_F \sqrt{n_{2D}}$, we plot $S_{xx}\sqrt{n_{2D}}$ (called β) vs T in the inset of Fig. 3(b). Extracted from the slope, v_F ranges from 0.8 to 1.7×10^6 m/s depending on the value of α (from 1 to 2), which is in good agreement with the values obtained by others [17]. In relating V_g to n_{2D} for above estimations, we use $n_{2D} = \frac{C_g V_g}{e} + \bar{n} = \frac{C_g}{e}(V_g - V_D)$, where C_g is the capacitance per unit area and \bar{n} is the induced density by charged impurities at the Dirac point. A value of $C_g = 103$ aF/ μm^2 is determined from our Hall data.

In a magnetic field, carriers diffusing under ∇T experience the Lorentz force, resulting in a nonzero transverse voltage V_y . The transverse effect or the Nernst effect is measured by $S_{xy} = -\frac{E_y}{|\nabla T|} = \frac{\Delta V_y}{\Delta T_x}$. In nonmagnetic metals, S_{xy} is negligibly small (~ 10 nV/K per tesla) [18]. In ferromagnets, spin-orbit coupling can lead to a large spontaneous Nernst signal [19]. Here, we observe an exceedingly large Nernst peak (~ 50 $\mu\text{V}/\text{K}$ at 8 T) at the Dirac point [Fig. 4(a)], and we attribute it to the unique band structure of graphene. In classical transport, the Mott relation takes the following form [7,20]: $S_{xy} = -\frac{\pi^2}{3} \frac{k_B^2 T}{e} \times (\frac{\partial \Theta_H}{\partial \mu})_\mu = \frac{\pi^2 k_B^2 T B}{3} \frac{\partial}{\partial \mu} [\frac{\tau}{m^*} \text{sgn}(\mu)]$. S_{xy} is directly proportional to the energy derivative of the Hall angle Θ_H or inversely proportional to the cyclotron mass m^* . For massless particles, the vanishing cyclotron mass can indeed lead to a

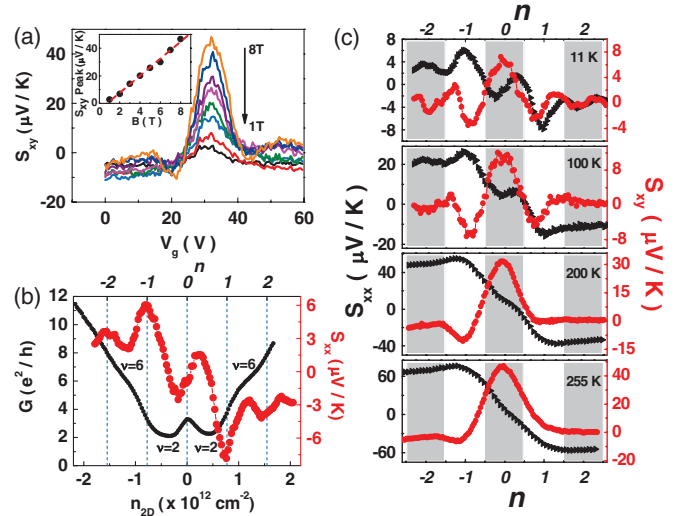


FIG. 4 (color). (a) V_g dependence of Nernst signal S_{xy} at 160 K with different magnetic fields (1–8 T). Inset: B dependence of S_{xy} at $V_g = V_D$, and the red line is a linear fit. (b) Two-terminal conductance G and thermopower S_{xx} vs carrier density n_{2D} at $T = 11$ K and $B = 8$ T. The corresponding Landau level index n is shown on the top axis. (c) S_{xx} (black triangle) and S_{xy} (red circle) vs Landau level index n for four different temperatures at $B = 8$ T.

diverging behavior in S_{xy} . In graphene devices, however, the anomaly is diminished by the impurity states near the Dirac point. Recall that the Mott relation breaks down in this region. Here, we estimate the magnitude of S_{xy} at the Dirac point both from Θ_H outside this region where the Mott relation holds and from γ . Since we have $\Theta_H = -\mu_c B \text{sgn}(\mu)$ (μ_c : carrier mobility), we obtain $\Delta\Theta_H \sim 2.2$ with an 8 T magnetic field at 255 K. This change in Θ_H occurs over $\gamma \sim 204$ meV as estimated from the width of the conductance minimum, yielding $S_{xy} \sim 68$ $\mu\text{V}/\text{K}$. This is in very good agreement with the experimentally observed peak value (~ 50 $\mu\text{V}/\text{K}$). Additionally, Θ_H is directly proportional to B , which indicates a linear B -field dependence in S_{xy} , with an estimated slope of ~ 5.4 $\mu\text{V}/\text{K}^*\text{T}$ at 160 K. Indeed, the linear B dependence of S_{xy} is observed [Fig. 4(a)], and the slope of the straight line is ~ 6 $\mu\text{V}/\text{K}^*\text{T}$. Similar to S_{xx} whose diverging behavior is greatly modified by the disorders, the anomaly in S_{xy} depends on the carrier mobility as well as γ . We expect to see more pronounced anomalous behavior in both S_{xx} and S_{xy} in cleaner samples.

At low temperatures and $B = 8$ T, the device conductance exhibits clear quantum Hall plateaus as V_g is varied. In this regime, we observe oscillations in S_{xx} [Figs. 4(b) and 4(c)] that are reminiscent of the Shubnikov–de Hass oscillations in ρ_{xx} [2,3], and the side peaks and dips in S_{xy} that correlate with the oscillatory structures in S_{xx} . At $T = 11$ K, S_{xx} shows peaks (dips) as μ is inside the broadened Landau levels (LL) on the hole (electron) side. These peaks (dips) correspond to the LL indices $n = 1$ and $n = 2$ for holes (electrons). S_{xy} also changes sign at these fillings. It is also worth noting that S_{xx} crosses zero at the Dirac point (in the lowest LL), accompanied by an additional small dip (peak) on the hole (electron) side. The origin of this feature is unknown, but it could reveal some peculiarities of the zeroth LL at high magnetic fields. In conventional 2D electron systems, the observed S_{xx} peaks at the LL's are consistent with the calculations in the integer quantum Hall regime [21]. In graphene samples, the $n = 1$ and $n = 2$ peaks in S_{xx} on both electron and hole sides are also expected. However, we do not observe vanishing S_{xx} as μ is located between the two adjacent LL's. The nonvanishing S_{xx} was previously attributed to the activated behavior in ordinary 2D electron systems. In our samples, the relatively large magnitude of S_{xx} between the LL's may be caused by the broadened LL's due to disorders. We expect to see $S_{xx} \rightarrow 0$ at low temperatures and the predicted activated behavior at high temperatures in cleaner samples.

As the temperature increases, the oscillations in S_{xx} and S_{xy} become weaker, although the overall magnitude of both S_{xx} and the central peak in S_{xy} increases [Fig. 4(c)]. As discussed earlier, the characteristic width of the Nernst peak is primarily determined by γ , which is greater than $k_B T$. The Nernst width remains nearly unchanged as a consequence.

In summary, the diverging behavior ($|S_{xx}| \sim 1/\sqrt{|n_{2D}|}$) of the Seebeck coefficient along with the exceedingly large Nernst peak at the Dirac point is characteristic of the massless particles in graphene. With disorders, these generic anomalies are somewhat masked near the Dirac point. However, the diverging behavior can be retrieved from those quantities as the chemical potential approaches the Dirac point. In higher mobility graphene samples, the anomalies are expected to be more drastically pronounced.

Authors would like to thank Chandra Varma for suggesting the thermopower study on graphene, and thank Chris Dames, Vivek Aji, Shan-Wen Tsai, and Vicent Ugarte for many helpful discussions. P. W., Y. P., and J. S. acknowledge the support of DOE DE-FG02-07ER46351 and ONR/DMEA H94003-07-2-0703. W. B. and C. N. L. acknowledge the support of NSF CAREER No. DMR/0748910, NSF No. CBET/0756359, and ONR/DMEA Grant No. H94003-07-2-0703.

Note added.—During the preparation of this manuscript, we became aware of related work with a similar conclusion from Zuev *et al.* [22].

-
- [1] K. S. Novoselov *et al.*, Science **306**, 666 (2004).
 - [2] K. S. Novoselov *et al.*, Nature (London) **438**, 197 (2005).
 - [3] Y. Zhang *et al.*, Nature (London) **438**, 201 (2005).
 - [4] V. P. Gusynin and S. G. Sharapov, Phys. Rev. Lett. **95**, 146801 (2005).
 - [5] A. H. Castro Neto *et al.*, Rev. Mod. Phys. **81**, 109 (2009).
 - [6] F. Miao *et al.*, Science **317**, 1530 (2007).
 - [7] V. P. Gusynin and S. G. Sharapov, Phys. Rev. B **73**, 245411 (2006).
 - [8] N. M. R. Peres, J. M. B. Lopes dos Santos, and T. Stauber, Phys. Rev. B **76**, 073412 (2007).
 - [9] B. Dora and P. Thalmeier, Phys. Rev. B **76**, 035402 (2007).
 - [10] J. P. Small, K. M. Perez, and P. Kim, Phys. Rev. Lett. **91**, 256801 (2003).
 - [11] S. Adam *et al.*, Proc. Natl. Acad. Sci. U.S.A. **104**, 18392 (2007).
 - [12] Y.-W. Tan *et al.*, Phys. Rev. Lett. **99**, 246803 (2007).
 - [13] K. I. Bolotin *et al.*, Phys. Rev. Lett. **101**, 096802 (2008).
 - [14] J. Martin *et al.*, Nature Phys. **4**, 144 (2008).
 - [15] N. M. R. Peres, F. Guinea, and A. H. Castro Neto, Phys. Rev. B **73**, 125411 (2006).
 - [16] T. Lofwander and M. Fogelstrom, Phys. Rev. B **76**, 193401 (2007).
 - [17] Z. Jiang *et al.*, Phys. Rev. Lett. **98**, 197403 (2007); Z. Q. Li *et al.*, Nature Phys. **4**, 532 (2008).
 - [18] J. A. Clayhold *et al.*, Phys. Rev. B **50**, 4252 (1994); Z. A. Xu *et al.*, Nature (London) **406**, 486 (2000).
 - [19] W.-L. Lee *et al.*, Phys. Rev. Lett. **93**, 226601 (2004); Y. Pu *et al.*, Phys. Rev. Lett. **101**, 117208 (2008).
 - [20] E. H. Sondheimer, Proc. R. Soc. A **193**, 484 (1948).
 - [21] H. Obloh, K. von Klitzing, and K. Ploog, Surf. Sci. **142**, 236 (1984); S. M. Girvin and M. Johnson, J. Phys. C **15**, L1147 (1982); M. Johnson and S. M. Girvin, Phys. Rev. B **29**, 1939 (1984).
 - [22] Y. M. Zuev *et al.*, Phys. Rev. Lett. **102**, 096807 (2009).